

Unbalanced OPF Modelling for Mixed Monopolar and Bipolar HVDC Grid Configurations

Chandra Kant Jat, *Member, IEEE*, Jay Dave, *Member, IEEE*, Dirk Van Hertem, *Senior Member, IEEE*,
Hakan Ergun, *Senior Member, IEEE*,

Abstract—HVDC is a critically important technology for the large-scale integration of renewable resources such as offshore wind farms. Currently, only point-to-point and multi-terminal HVDC connections exist in real-life operation. However, with the advancement of VSC-based converter technologies, future HVDC systems are foreseen to develop into meshed HVDC grids. Bipolar HVDC grids can be operated in an unbalanced way during single pole outages or in form of mixed monopolar and bipolar grids. However, currently, there are no (optimal) power flow tools to study the feasibility of such systems. Therefore, we develop an optimal power flow (OPF) model for hybrid AC-DC grids to capture the DC side unbalances and allowing to efficiently plan and operate such future grids. In this paper, we present a multi-conductor OPF model with separate modeling of the positive pole, negative pole, metallic return conductors, and ground return. The capabilities of the model are demonstrated on a small test case, including monopolar tapping over a bipolar DC link. It is demonstrated that the developed OPF model can capture the loop flows between the different poles in unbalanced conditions, as opposed to the existing single-wire representations in the literature. Further, numerical results are presented for multiple test cases with various system sizes, starting from an 11-bus system to a 3120-bus system to demonstrate the computational tractability of the chosen model formulation.

Index Terms—HVDC transmission, hybrid AC/DC grids, meshed HVDC grids, optimal power flow, power system modeling

I. INTRODUCTION

A. Background and literature review

The High Voltage Direct Current (HVDC) technology has traditionally been used for long-distance power transmission, connections of two asynchronous areas, and under-ground/sub-sea transmission links, mostly as point-to-point connections or a few multi-terminal links. Although most present-day HVDC links are based on LCC converter technology, with recent advancements in Voltage Source Converters (VSC) and the latest developments in DC protection, meshed HVDC grids have become viable options for the future power systems [1], [2]. Many studies show that interconnection of different countries and remote offshore wind farms using HVDC is grids is the techno-economically most viable option [3]–[5].

Power flow and optimal power flow models allow to investigate the feasibility and to quantify the benefits of new

operational concepts. In the context of hybrid AC/DC networks, several formulations exist to solve the Optimal Power Flow (OPF) problem [6]–[9]. A sequential AC/DC power flow algorithm is discussed in [6] that is further developed as a Matlab-based open-source tool in [10], whereas [7] and [8] present AC/DC OPF models for VSC-based meshed DC grids. Gan et al. [9] present a second-order cone programming relaxation for the OPF problem in DC networks. Meyer et al. [11] present a distributed OPF problem for hybrid AC/DC grids, using an improved alternating direction of multipliers method (ADMM) as well as augmented Lagrangian based alternating direction inexact Newton (ALADIN) method. The authors in [12] present a robust optimization model for the AC/DC grids while including uncertainty. Hotz et. al. [13] describe a python-based open-source OPF framework for mixed AC/DC grids incorporating only point-to-point and radially connected multi-terminal DC networks. Recently, a comprehensive combined AC/DC OPF model, including meshed HVDC systems, is presented in [14] which models converter stations with transformers, filters, and phase reactors in detail. Different approximations and relaxations of the non-linear optimization problem are also discussed. However, all the above-mentioned works model the DC grid as a balanced system using a single conductor representation. None of them model the metallic return conductor explicitly.

These single-conductor representations are based on the assumption that the DC grid consists of homogeneous HVDC configurations, meaning that they are carried out either as monopolar or as bipolar networks, as shown in Fig. 1. In the case of a monopolar DC grid, the converters and lines can have exclusively either symmetric or asymmetric configurations. Additionally, for bipolar HVDC grids, the single-conductor models assume a balanced operating state, i.e., no current flows through metallic or ground return, the same amount of power flows through the two poles of a converter, and the neutral point voltage is zero.

However, the existing literature on HVDC suggests that a mix of monopolar and bipolar HVDC links can help find grid designs with reduced investment costs without compromising reliability [15]–[17]. Moreover, with the possibility of operating the HVDC grid in unbalanced conditions, e.g. asymmetric operation of the HVDC grid, a single pole contingency at a bipolar converter station would not cause a complete terminal outage. Thus, the availability of the DC grid [18] is improved. However, the unbalanced utilization of the positive and negative poles can cause a shift of the metallic return conductor voltage, which needs to be limited. The actual nodal

This paper has received support from the NEPTUNE project, the Belgian Energy Transition fund (Corresponding author: Chandra Kant Jat.)

The authors are with the Research Group ELECTA, Department of Electrical Engineering, Katholieke Universiteit, Leuven 3000 Leuven, Belgium, and also with EnergyVille 3600 Genk, Belgium (e-mail: chandrakant.jat@kuleuven.be).

voltages of the poles and metallic return depend not only on the power injections/flows in the DC grid but also on the different grounding configurations chosen at the various converter stations (Fig. 1b).

To analyze the implications of unbalanced utilization of bipolar HVDC grids, an (optimal) power flow model is needed, which can explicitly model the DC grid unbalance. Using such an optimal power flow model, optimal positive and negative pole voltage and power set points for the HVDC converter stations can be determined for unbalanced operation while respecting AC and DC grid constraints such as current and voltage limits. In particular, it can be guaranteed that the metallic return conductor voltage does not exceed defined safety limits for various operating conditions that can occur due to the variability of renewable generation sources.

Although the multi-conductor representation of power networks is highly investigated in the context of unbalanced low voltage AC networks [20]–[23], the unbalanced operation of HVDC networks is not investigated widely. At the same time, high-voltage AC networks are generally represented by single conductor models because the amount of unbalance among the three phases is often negligible. For asymmetric HVDC grid operation, e.g., after single pole outages of bipolar HVDC links, an unbalance of 50% with respect to the nominal power of the link can occur. Thus, accurately capturing the imbalance is essential for the operation of asymmetric HVDC grids. Authors in [24] and [25] explicitly model metallic return for bipolar grids having asymmetric loading conditions; however, with a scope limited only to DC systems, e.g. DC-DC

converter stations. Thus, to the authors' knowledge, a complete multi-conductor AC/DC OPF model for analyzing unbalanced or asymmetric HVDC grid operation does not exist in the literature.

B. Contributions and outline

This paper develops an optimal power flow model for unbalanced mixed monopolar/bipolar HVDC networks where both poles of bipolar converters, the transmission line, and the metallic return conductors are explicitly modeled. The grounding impedance of the HVDC converter stations, e.g. rigid grounding versus high impedance grounding, is taken into account, such that the correct voltage profile of the metallic return conductor is obtained and can be used as an optimization constraint. The AC network is modeled as a balanced network, as voltage unbalance is usually negligible in high-voltage AC networks. The HVDC converters are modeled generically, including converter station transformers, harmonic filters, and converter losses as described in [14]. The power-voltage (P-V) formulation, which is the most common formulation for OPF problems, fails to capture nodal-current balance in the neutral terminal and causes numerical issues due to the low magnitude of the neutral conductor voltage. Therefore, the DC grid is modeled in terms of voltage and current variables, i.e. the I-V formulation. The developed optimization model is implemented as an extension of the open source 'PowerModelsACDC.jl' package [26], developed in Julia/JuMP [27] and uses the well-known 'PowerModels.jl' package [28] for the modelling of the balanced AC system. The multi-conductor modeling functionality is inspired by the models included in the package 'PowerModelsDistribution.jl' [29]. The paper's contributions with respect to the existing literature are shown in table I.

The paper is outlined as follows. An OPF problem with the objective of generation cost minimization is introduced in section II. The AC/DC grid model, including the multi-conductor DC grid representation, is described in Section III. Section IV provides numerical results for a small test case and validates the developed model, whereas section V presents numerical results for larger test cases quantifying computation performance. Finally, conclusions are presented in Section VI.

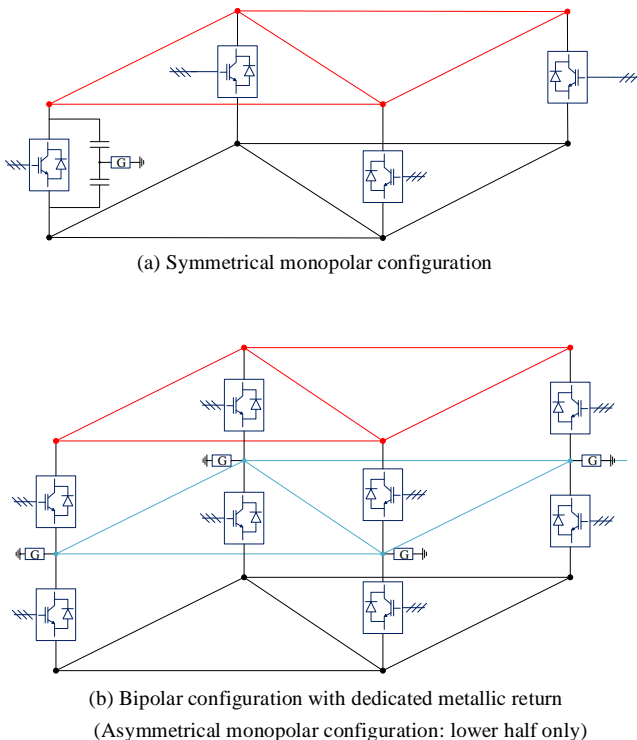


Fig. 1. HVDC grid configurations and grounding options [19]

TABLE I
CONTRIBUTION

	AC/DC systems including AC/DC converter	Unbalanced DC side model metallic or ground return	monopolar & bipolar converter	open -source tool
[6]–[9]	✓	✗	✗	✗
[10], [13], [14]	✓	✗	✗	✓
[24], [25]	✗	✓	✓	✗
This paper	✓	✓	✓	✓

II. PROBLEM FORMULATION

The power flow model presented in this paper is generally valid for different power system optimization objectives such as generation cost minimization, transmission loss minimization, etc. In this work we use a generation cost minimization

objective as shown in (1) and the general constraints are shown throughout (2) - (11), which are explained in detail in the following paragraphs.

$$\min \sum_{g \in \mathcal{G}} a_g + b_g P_g + c_g P_g^2, \quad (1)$$

subject to

$$U_i^{\min} \leq U_i \leq U_i^{\max} \quad \forall i \in \mathcal{I} \quad (2)$$

$$U_{e\phi}^{\text{dc,max}} \leq U_{e\phi}^{\text{dc}} \leq U_{e\phi}^{\text{dc,max}} \quad \forall e \in \mathcal{E} \quad (3)$$

$$\theta_r = 0 \quad \forall r \in \mathcal{R} \quad (4)$$

$$P_{\min} \leq P_g \leq P_{\max} \quad \forall g \in \mathcal{G} \quad (5)$$

$$Q_{\min} \leq Q_g \leq Q_{\max} \quad \forall g \in \mathcal{G} \quad (6)$$

$$\text{AC branch flow constraint} \quad (7)$$

$$\text{DC branch flow constraint} \quad (8)$$

$$\text{AC bus KCL constraint} \quad (9)$$

$$\text{DC bus KCL constraint} \quad (10)$$

$$\text{AC/DC conversion constraint} \quad (11)$$

The objective function (1), e.g., the active power generation costs are expressed as a quadratic cost function, where a_g , b_g and c_g are the corresponding cost coefficients. Equations (2) and (3) represent the AC and the DC side voltage limits, respectively, while (4) fixes the nodal voltage angles for the reference bus(es). Active and reactive power limits of the generators are enforced in (5) and (6). Equations (7) to (11) enforce the line flow limits, nodal current balance in AC and DC nodes, and the power flow constraints and technical limits associated with AC/DC converter stations. The sets and indices used throughout the paper are introduced in table II whereas table III presents variables and parameters of the DC grid. The well known non linear, non convex equations for modeling the balanced AC network are incorporated using the open-source tool presented in [28].

TABLE II
DEFINITION OF AC/DC OPF ENTITIES, INDICES, AND SETS

ac nodes	$i, j \in \mathcal{I}$
ac branches	$l \in \mathcal{L}$
ac topology	$lij \in \mathcal{T}^{\text{ac}} \subseteq \mathcal{L} \times \mathcal{I} \times \mathcal{I}$
dc nodes	$e, f \in \mathcal{E}$
dc subnodes or subbranches	$\phi \in \{1, 2, 0\}$
dc branches	$d \in \mathcal{D}$
dc topology	$def \in \mathcal{T}^{\text{dc}} \subseteq \mathcal{D} \times \mathcal{E} \times \mathcal{E}$
AC/DC converters	$c \in \mathcal{C}$
converter pole	$\rho \in \{1, 2\}$
AC/DC converter topology	$cie \in \mathcal{T}^{\text{cv}} \subseteq \mathcal{C} \times \mathcal{I} \times \mathcal{E}$
generators	$g \in \mathcal{G}$
reference ac buses	$r \in \mathcal{R}$
loads	$m \in \mathcal{M}$
ac generator connectivity	$gi \in \mathcal{T}^{\text{gen,ac}} \subseteq \mathcal{G} \times \mathcal{I}$
ac load connectivity	$mi \in \mathcal{T}^{\text{load,ac}} \subseteq \mathcal{M} \times \mathcal{I}$
dc load connectivity	$me \in \mathcal{T}^{\text{load,dc}} \subseteq \mathcal{M} \times \mathcal{E}$

III. AC/DC GRID MODEL

A static power flow model for the hybrid AC/DC power system is described in this section, extending the AC network equations presented in [28]. Although this paper's contribution lies in modeling of unbalanced DC grid, AC side modeling is

TABLE III
DC SIDE PARAMETERS AND VARIABLES

Current flow over DC branch	$I_{e\phi}^{\text{dc}}$
Power loss in the DC line	$P_{\text{loss}}^{\text{dc}}$
Current rating in the DC line	$I_{e\phi}^{\text{dc,rated}}$
Bus voltage magnitude	U_e^{dc}

also presented to show the impact of multi-conductor modeling of AC/DC converter on the AC side and to present a complete picture of the system under consideration.

A. Static AC grid model

The AC grid is modeled as a balanced system with power flow equations in the power-voltage formulation, as described in [31]. The active and reactive power flow through line l between node i and j is calculated as

$$P_{lij}^{\text{ac}} = g \cdot (U_i^{\text{mag}2} - U_i^{\text{mag}} U_j^{\text{mag}} \cdot \cos(\theta_i - \theta_j)) - b \cdot (U_i^{\text{mag}} \cdot U_j^{\text{mag}} \cdot \sin(\theta_i - \theta_j)) \quad \forall lij \in \mathcal{T}^{\text{ac}} \quad (12)$$

$$Q_{lij}^{\text{ac}} = -b \cdot (U_i^{\text{mag}2} - U_i^{\text{mag}} \cdot U_j^{\text{mag}} \cdot \cos(\theta_i - \theta_j)) - g \cdot (U_i^{\text{mag}} \cdot U_j^{\text{mag}} \cdot \sin(\theta_i - \theta_j)) \quad \forall lij \in \mathcal{T}^{\text{ac}} \quad (13)$$

Where the line admittance is given represented as $y_{ij} = g + j \cdot b$. For more details, the readers are referred to the package at [28], which is directly invoked in the proposed model. The nodal active and reactive balance equations on AC grid nodes $i \in \mathcal{T}^{\text{ac}}$ are defined as:

$$\begin{aligned} & \sum_{cie \in \mathcal{T}^{\text{cv}}, \rho \in \{1, 2\}} P_{c\rho ie\rho}^{\text{tf}} + \sum_{lij \in \mathcal{T}^{\text{ac}}} P_{lij}^{\text{ac}} \\ &= \sum_{gi \in \mathcal{T}^{\text{gen,ac}}} P_g - \sum_{mi \in \mathcal{T}^{\text{load,ac}}} P_m - g_i^{\text{shunt}} (U_i^{\text{mag}})^2 \quad \forall i \in \mathcal{I}, \quad (14) \\ & \sum_{cie \in \mathcal{T}^{\text{cv}}, \rho \in \{1, 2\}} Q_{c\rho ie\rho}^{\text{tf}} + \sum_{lij \in \mathcal{T}^{\text{ac}}} Q_{lij}^{\text{ac}} \\ &= \sum_{gi \in \mathcal{T}^{\text{gen,ac}}} Q_g - \sum_{mi \in \mathcal{T}^{\text{load,ac}}} Q_m + b_i^{\text{shunt}} (U_i^{\text{mag}})^2 \quad \forall i \in \mathcal{I} \quad (15) \end{aligned}$$

Where P_g , P_m , Q_g , and Q_m represent the active and reactive power set points of generators and loads, respectively, similarly, $g_i^{\text{shunt}} + j b_i^{\text{shunt}}$ is the shunt admittance connected to the AC bus.

B. Static DC grid model

A generic HVDC grid can have a mix of different configurations as shown in Fig. 2, originally presented in [30]. It can be seen that all the different configurations consist of either one or two converter poles and either two or three conductors for DC branches. All other configurations can be represented as a subset of the bipolar converter and DC branch configurations. Therefore, the following equations are described in the context of a bipolar converter station and a bipolar HVDC link with a metallic return.

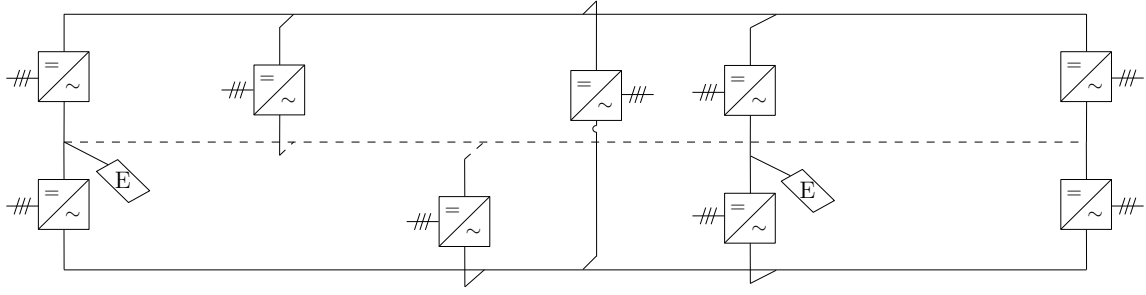


Fig. 2. An HVDC grid with a different mix of converter and line configurations (in fact, it is a multi-terminal system that can be easily extended into a meshed system). It presents a variety of tapping (two asymmetric monopoles, one symmetric monopolar, and one bipolar with ground return) on a bipolar link with metallic return [30]

Since DC the grid is modeled in the I-V formulation, Kirchhoff's current law at each DC node is modeled using current variables ($\forall \phi \in \{1, 2, 0\}$):

$$\sum_{cie \in \mathcal{T}^{\text{cv}}} I_{c\rho}^{\text{cv,dc}} + \sum_{cie \in \mathcal{T}^{\text{cv}}} I_{c_g}^{\text{cv,dc}} + \sum_{def \in \mathcal{T}^{\text{dc}}} I_{d^\phi e^\phi f^\phi}^{\text{dc}} = 0 \quad \forall e \in \mathcal{E} \quad (16)$$

where $I_{c\rho}^{\text{cv,dc}}$ is the DC converter current in pole ρ connected to DC node e , and $I_{c_g}^{\text{cv,dc}}$ is the converter ground current modeled as a shunt current at the neutral terminal. $I_{d^\phi e^\phi f^\phi}^{\text{dc}}$ is the current of DC branch d connecting the DC nodes e and f .

All conductors of the DC branch (i.e., positive, negative and return conductor) are modeled separately as shown in Fig. 3, where r_d is the resistance of positive pole and negative pole conductors and r_{d0} is the resistance of return conductor.

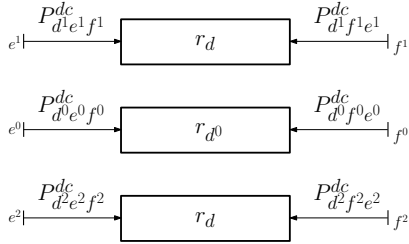


Fig. 3. Multi-conductor static model for bipolar DC branch

The DC grid is modeled using current and voltage variables, i.e., the I-V formulation. This choice over the commonly used P-V (power-voltage) formulation for the AC grid ensures that Kirchhoff's current law (KCL) at the neutral terminal is met. For near zero values (below numerical accuracy, e.g. tolerance of the optimization solver) of the voltage V at a node, the value for power $P = V \cdot I$ also takes near zero values, thus violating the current balance in the node.

The DC branch power flow model in terms of the current variable is defined as

$$I_{d^\phi e^\phi f^\phi}^{\text{dc}} + I_{d^\phi f^\phi e^\phi}^{\text{dc}} = 0 \quad \forall def \in \mathcal{T}^{\text{dc}}. \quad (17)$$

where $I_{d^\phi e^\phi f^\phi}^{\text{dc}}$ is the current flow in conductor ϕ of line d in direction from node e to f . $I_{d^\phi f^\phi e^\phi}^{\text{dc}}$ is the current in the opposite direction. The current flow for the multi-conductor line can be defined as:

$$I_{d^\phi e^\phi f^\phi}^{\text{dc}} = (1/r_{d^\phi}) \cdot (U_{e^\phi}^{\text{dc}} - U_{f^\phi}^{\text{dc}}) \quad \forall def \in \mathcal{T}^{\text{dc}} \cup \mathcal{T}^{\text{dc,rev}} \quad (18)$$

where r_{d^ϕ} is the resistance of conductor ϕ of DC line d . $\mathcal{T}^{\text{dc,rev}}$ is DC topology with reverse order of nodes. It is used to apply the same equation for the opposite direction of current (or power) flow.

The branch current is constrained by the branch current limits:

$$-I_{d^\phi}^{\text{dc, rated}} \leq I_{d^\phi e^\phi f^\phi}^{\text{dc}} \leq I_{d^\phi}^{\text{dc, rated}} \quad \forall def \in \mathcal{T}^{\text{dc}} \cup \mathcal{T}^{\text{dc,rev}} \quad (19)$$

C. Static AC/DC converter station model

The generic AC/DC converter station model is composed of a power-electronic AC/DC converter, a phase reactor as a series impedance, a filter as a shunt susceptance, and a transformer represented with a tap ratio t_c and a series impedance. The readers are referred to [14] for the details of the transformer, phase reactor, filter, and power electronic converter equations. These equations have been modified in this paper for the multi-conductor model.

Fig. 4 depicts the bipolar converter station model and associated optimization variables. As shown in Fig. 4, a bipolar converter station has two separate AC connections, one for the positive pole ($\rho = 1$) and one for the negative pole ($\rho = 2$). The DC side of the converter has three connections, namely, the positive pole ($\phi = 1$), the negative pole ($\phi = 2$), and the neutral/earth ($\phi = 0$) terminal. The AC side voltage is complex-valued, i.e., $U_i = U_i^{\text{mag}} \angle \theta_i$, whereas the DC side voltage is real-valued represented by the voltage magnitude $U_{e^\phi}^{\text{dc}}$. In addition, two internal AC voltages are present at the filter connection point, $U_{c\rho}^f = U_{c\rho}^{\text{f, mag}} \angle \theta_{c\rho}^f$, and at the power-electronic converter $U_{c\rho}^{\text{cv}} = U_{c\rho}^{\text{cv, mag}} \angle \theta_{c\rho}^{\text{cv}}$. As described in [14], any phase shift over the converter transformer is just an offset to the two internal AC voltages w.r.t. the AC bus voltage. The following paragraphs describe the different building blocks of the converter station model.

1) *AC/DC converter*: The apparent converter power is defined through the circle constraints and bound by active, reactive and apparent power limits ($\forall \rho \in \{1, 2\}$):

$$(P_{c\rho}^{\text{cv,ac}})^2 + (Q_{c\rho}^{\text{cv,ac}})^2 \leq (S_{c\rho}^{\text{cv,ac, rated}})^2 \quad \forall cie \in \mathcal{T}^{\text{cv}}, \quad (20)$$

$$(P_{c\rho}^{\text{cv,ac}})^2 + (Q_{c\rho}^{\text{cv,ac}})^2 = (U_{c\rho}^{\text{cv, mag}})^2 (I_{c\rho}^{\text{cv, mag}})^2 \quad \forall cie \in \mathcal{T}^{\text{cv}} \quad (21)$$

$$P_{c\rho}^{\text{cv,ac, min}} \leq P_{c\rho}^{\text{cv,ac}} \leq P_{c\rho}^{\text{cv,ac, max}} \quad \forall cie \in \mathcal{T}^{\text{cv}}, \quad (22)$$

$$Q_{c\rho}^{\text{cv,ac, min}} \leq Q_{c\rho}^{\text{cv,ac}} \leq Q_{c\rho}^{\text{cv,ac, max}} \quad \forall cie \in \mathcal{T}^{\text{cv}}, \quad (23)$$

$$U_c^{\text{cv, min}} \leq U_{c\rho}^{\text{cv, mag}} \leq U_c^{\text{cv, max}} \quad \forall cie \in \mathcal{T}^{\text{cv}}. \quad (24)$$

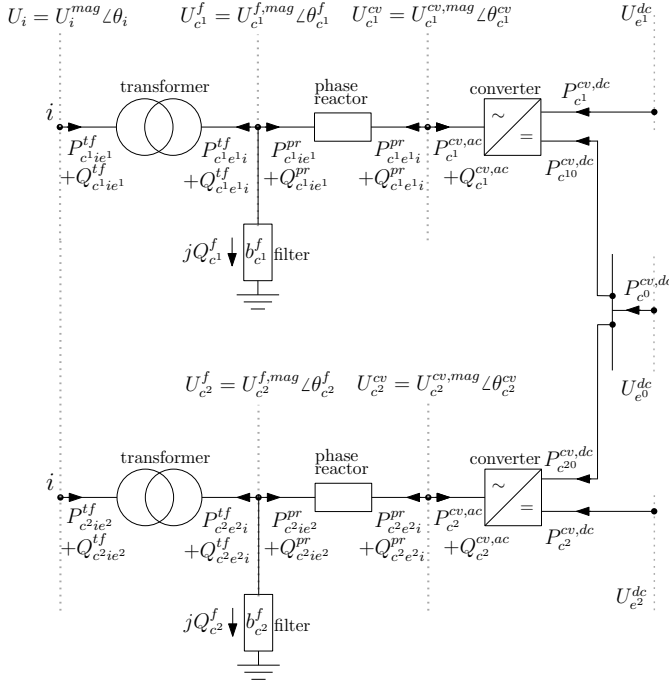


Fig. 4. Overview of the converter station model

Active power injected/absorbed by the converter into/from the DC grid is modeled by the variable $P_{c\rho}^{cv,dc}$ as shown in Fig. 4. This power is bound to operational limits as

$$P_{c\rho}^{cv,dc,\min} \leq P_{c\rho}^{cv,dc} \leq P_{c\rho}^{cv,dc,\max} \quad \forall cie \in \mathcal{T}^{cv}. \quad (25)$$

The AC and DC side power injections of the converter poles are linked using the converter losses:

$$P_{c\rho}^{cv,ac} + P_{c\rho}^{cv,dc} + P_{c0}^{cv,dc} = P_{c\rho}^{cv,\text{loss}} \quad \forall cie \in \mathcal{T}^{cv}. \quad (26)$$

Where $P_{c10}^{cv,dc}$ and $P_{c20}^{cv,dc}$ represent the power flow between the positive and negative poles and the neutral terminal, respectively. $P_{c1}^{cv,\text{loss}}$ and $P_{c2}^{cv,\text{loss}}$ are the losses of the positive and negative poles of the converter and are defined as,

$$P_{c\rho}^{cv,\text{loss}} = a_{c\rho}^{cv} + b_{c\rho}^{cv} \cdot I_{c\rho}^{cv,\text{mag}} + c_{c\rho}^{cv} \cdot (I_{c\rho}^{cv,\text{mag}})^2 \quad \forall cie \in \mathcal{T}^{cv}. \quad (27)$$

In (27), $I_{c\rho}^{cv,\text{mag}}$ is the AC side current magnitude of pole ρ of the converter c . This current is constrained by the converter's current rating $I_{c\rho}^{cv,\text{rated}}$ for each pole $\rho \in \{1, 2\}$:

$$I_{c\rho}^{cv,\text{mag}} \leq I_{c\rho}^{cv,\text{rated}} \quad \forall cie \in \mathcal{T}^{cv}. \quad (28)$$

DC side converter current is linked to the DC side power injection using (29) is bound by the current rating $I_{c\rho}^{cv,dc,\max}$ using (30).

$$P_{c\rho}^{cv,dc} = U_{e\rho}^{dc} \cdot I_{c\rho}^{cv,dc,\text{mag}} \quad \forall cie \in \mathcal{T}^{cv}, \quad (29)$$

$$I_{c\rho}^{cv,dc,\min} \leq I_{c\rho}^{cv,dc,\text{mag}} \leq I_{c\rho}^{cv,dc,\max} \quad \forall cie \in \mathcal{T}^{cv}. \quad (30)$$

2) *Transformer*: The active and reactive power seen at the AC bus i of the converter transformer of pole ρ of converter c are defined as:

$$P_{c\rho ie\rho}^{tf} = g_{c\rho}^{tf} \left(\frac{U_i^{\text{mag}}}{t_{c\rho}} \right)^2 - g_{c\rho}^{tf} \frac{U_i^{\text{mag}}}{t_{c\rho}} U_{c\rho}^{f,\text{mag}} \cos(\theta_i - \theta_{c\rho}^f) - b_{c\rho}^{tf} \frac{U_i^{\text{mag}}}{t_{c\rho}} U_{c\rho}^{f,\text{mag}} \sin(\theta_i - \theta_{c\rho}^f) \quad \forall cie \in \mathcal{T}^{cv} \cup \mathcal{T}^{cv,\text{rev}}, \quad (31)$$

$$Q_{c\rho ie\rho}^{tf} = -b_{c\rho}^{tf} \left(\frac{U_i^{\text{mag}}}{t_{c\rho}} \right)^2 + b_{c\rho}^{tf} \frac{U_i^{\text{mag}}}{t_{c\rho}} U_{c\rho}^{f,\text{mag}} \cos(\theta_i - \theta_{c\rho}^f) - g_{c\rho}^{tf} \frac{U_i^{\text{mag}}}{t_{c\rho}} U_{c\rho}^{f,\text{mag}} \sin(\theta_i - \theta_{c\rho}^f) \quad \forall cie \in \mathcal{T}^{cv} \cup \mathcal{T}^{cv,\text{rev}}. \quad (32)$$

where $g_{c\rho}^{tf}$ and $b_{c\rho}^{tf}$ are the conductance and susceptance of the converter transformers for the ρ^{th} pole, respectively. $t_{c\rho}$ is the converter transformer tap changer setting.

3) *Capacitive filter*: The reactive power of the filter capacitor of pole ρ of the converter c is calculated as:

$$Q_{c\rho}^f = -b_{c\rho}^f (U_{c\rho}^{f,\text{mag}})^2 \quad \forall cie \in \mathcal{T}^{cv}. \quad (33)$$

4) *Phase reactor*: The phase reactor impedance is defined as $z_{c\rho}^{\text{pr}} = r_{c\rho}^{\text{pr}} + jx_{c\rho}^{\text{pr}}$, with the equivalent admittance $y_{c\rho}^{\text{pr}} = \frac{1}{z_{c\rho}^{\text{pr}}} = g_{c\rho}^{\text{pr}} + jb_{c\rho}^{\text{pr}}$. As both the transformer and the reactor are modeled as a series impedance, for modeling the phase reactor equations (31) - (32) can be used by choosing $t_{c\rho} = 1$ and using the respective voltage variables and angles according to Fig. 4.

The active and reactive power balance at the node connecting the transformer, the filter capacitor, and the phase reactor is defined as:

$$P_{c\rho ie\rho}^{\text{pr}} + P_{c\rho ie\rho}^{tf} = 0 \quad \forall cie \in \mathcal{T}^{cv}, \quad (34)$$

$$Q_{c\rho ie\rho}^{\text{pr}} + Q_{c\rho ie\rho}^{tf} + Q_{c\rho}^f = 0 \quad \forall cie \in \mathcal{T}^{cv}. \quad (35)$$

5) *Converter DC side current constraints*: Fig. 5 shows an individual pole representation of the DC side of a bipolar converter station. For converter c , the superscripts 1 and 2 indicate positive and negative poles, respectively, whereas 0 indicates the neutral. To ensure the numerical stability of the optimization problem, the DC side converter currents need to be modeled explicitly. Since, the power-only representation fails to model the system accurately due to the low, neutral voltage, e.g., for low-impedance grounding on the DC side. The DC side converter's current constraints are

$$I_{c1}^{cv,dc} + I_{c10}^{cv,dc} = 0, \quad (36)$$

$$I_{c2}^{cv,dc} + I_{c20}^{cv,dc} = 0, \quad (37)$$

$$I_{c0}^{cv,dc} = I_{c10}^{cv,dc} + I_{c20}^{cv,dc}, \quad (38)$$

$$I_{c1}^{cv,dc} + I_{c2}^{cv,dc} + I_{c0}^{cv,dc} = 0. \quad (39)$$

Equations (36) and (37) imply that the DC current entering each pole should be equal to the current exiting. Equation (38) defines the net current in the neutral conductor, and (39) states that the difference of positive and negative pole currents must solely flow through the neutral conductor.

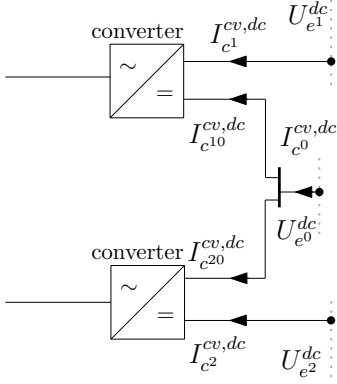


Fig. 5. Visualisation of the converter current constraints

6) *DC grid grounding constraint*: DC grid is modeled in the most generic way allowing multiple grounding points. Although theoretically possible [30], the use of the ground as a return in HVDC operation is not permitted in many parts of the world [19]. In this model, ground return operation has been included for the sake of generality. The ground is modeled as a superconducting plane, whereas the impedance of the ground return path is lumped at the grounding terminals. Thus, the ground is represented as a shunt element connected at the neutral terminal of the respective DC bus. The grounding impedance in the steady state DC model is effectively a resistance. It is indicated by the red color in Fig. 7. In this model, the option of grounding is considered only at the DC buses with converter stations which can be easily extended to other buses. The grounding current is defined as

$$I_{c_g}^{cv,dc} = \frac{U_{e^0}^{dc}}{r_g} \quad \forall c \in \mathcal{C}. \quad (40)$$

where $U_{e^0}^{dc}$ is neutral terminal voltage magnitude of DC bus e to which converter c is connected and r_g is the grounding resistance.

IV. TEST CASE AND NUMERICAL RESULTS

This section presents the impact of the multi-conductor modeling that can capture unbalanced loading conditions of DC grids. The test case and numerical results are as follows.

A. Test case

The test case consists of 3 AC systems interconnected through an HVDC system, as shown in Fig. 6. AC grid 1 and AC grid 2 are two identical 5-bus systems, each with two generators. They are connected to the DC grid through bipolar converter stations Conv-1 and Conv-2, respectively. AC grid 3 is a single bus system with a generator and a load at the same bus. Its connection to the DC grid is through Conv-3, which has an asymmetric monopolar configuration. This monopolar converter is connected to the bipolar link through a monopolar tapping at the negative and neutral terminals of DC bus 4. In this test case, the generation costs are modified such that AC grid 1 is the cheapest zone, whereas AC grid 3 is the costliest one. Thus, it can be expected that the OPF solution

results in export from AC grid 1 and import to AC grid 3. The exact multi-conductor representation of the DC side of this test system is presented in Fig. 7. All results presented throughout the tables are in per unit (pu) for power, current, and voltages, whereas it is USD (\$) for the objective function unless specified otherwise. The power base is 100 MVA , whereas the voltage base is 345 kV .

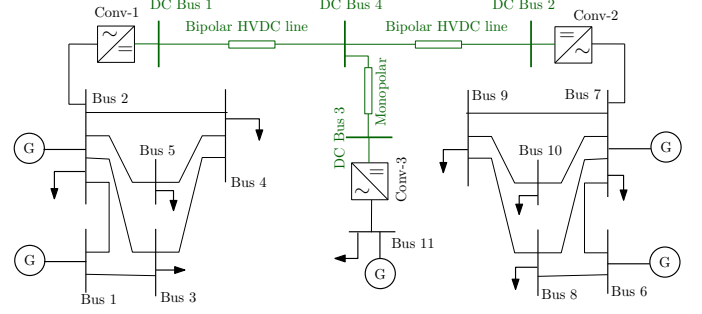


Fig. 6. Single line diagram of the test case

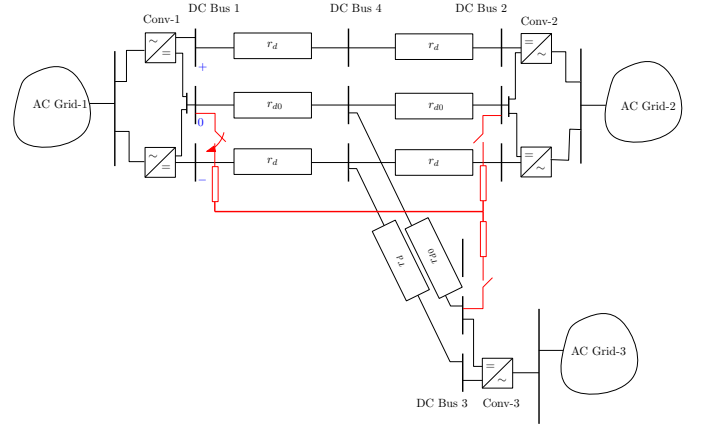


Fig. 7. Circuit diagram of the unbalanced DC network used in the test case. The red connections indicate the grounding impedances.

B. Validation against existing balanced formulations

Since there are no pre-existing benchmark models and test cases for unbalanced AC/DC networks, direct validation is not possible. A balanced network is an edge case of a generic unbalanced network, and thus, it can be used to validate the model indirectly. As the proposed multi-conductor model can equally be applied to balanced networks, its output has been compared to the balanced AC/DC OPF model of the PowerModelsACDC.jl package [26].

If Conv-3 and the monopolar link (between DC buses 3 and 4) in the test case (Fig. 7) are converted to bipolar configurations, the resulting network becomes a balanced bipolar HVDC system which can be solved using both the balanced and unbalanced multi-conductor models. By solving a generation cost minimization OPF problem using both models, it is found that the values of the objective function and generator set points match up to the solver's numerical accuracy ($1e-6$). Both AC and DC side branch flows and bus voltages are found

to be the same. The converter power flows and DC grid voltage magnitudes are presented in Table IV where *ACDC* refers to the solution obtained with the balanced single-conductor OPF model, and *MCDC* refers to the results obtained with the proposed multi-conductor model. As expected, we can see that the converter powers are equally divided between both poles. Positive and negative terminal voltages are equal for each DC bus, while the neutral voltage is zero. Thus, it can be concluded the proposed *MCDC* model, with the detailed representation of the DC side, finds correct solutions.

TABLE IV
COMPARING *ACDC* AND *MCDC* RESULTS FOR BALANCED SYSTEM

		DC bus voltage magnitude			
		Bus 1	Bus 2	Bus 3	Bus 4
<i>ACDC</i>	Positive	1.1	1.08134	1.07565	1.08566
<i>MCDC</i>	Negative	-1.1	-1.08134	-1.07565	-1.08566
	Neutral	0.000	0.000	0.000	0.000
		DC side power injections (MW)			
		Conv-1	Conv-2	Conv-3	
<i>ACDC</i>		62.53	-16.80	-40.00	
<i>MCDC</i>	Positive Pole	31.27	-8.40	-20.00	
	Negative pole	31.27	-8.40	-20.00	

C. Unbalanced OPF using balanced OPF tool

In this section, an attempt is made to solve the original unbalanced test case with the already existing balanced OPF tool *ACDC*. The solution of the system under consideration with this balanced model results in the net power exchange as indicated in the first row of Table V. For the individual pole flows, such models rely on equally dividing the bipolar converter power to both poles (2nd and 3rd rows of Table V). Although a solution is found by the optimizer because equal power division between the converter station poles is assumed, the obtained solution is infeasible in reality. This is shown in Fig. 8, where the black arrows indicate the solution obtained by the balanced model. Due to the assumption of equal power sharing, the obtained solution of the balanced model does not respect the nodal power balance at positive and negative terminals of DC bus 4 (highlighted with red dashed lines). Since the monopolar link is connected to the negative and neutral conductors of the bipolar link, both poles of Conv-1 and Conv-2 would not be loaded equally. This phenomenon can not be captured by balanced AC/DC OPF models. Although the single conductor *ACDC* model accurately captures the net power exchanges between the AC and DC grid, it fails to make an appropriate allocation of the power set points of each converter pole in operation. Thus, explicit representation of each converter pole and DC link conductor is essential.

D. Unbalanced OPF using the multi-conductor model

In this case, the OPF problem is solved using the proposed multi-conductor AC/DC OPF model (*MCDC*). The generator set-points obtained by the single conductor (*ACDC*) and the multi-conductor models are compared in Table VI. It can be observed that the generator set-points are the same in both

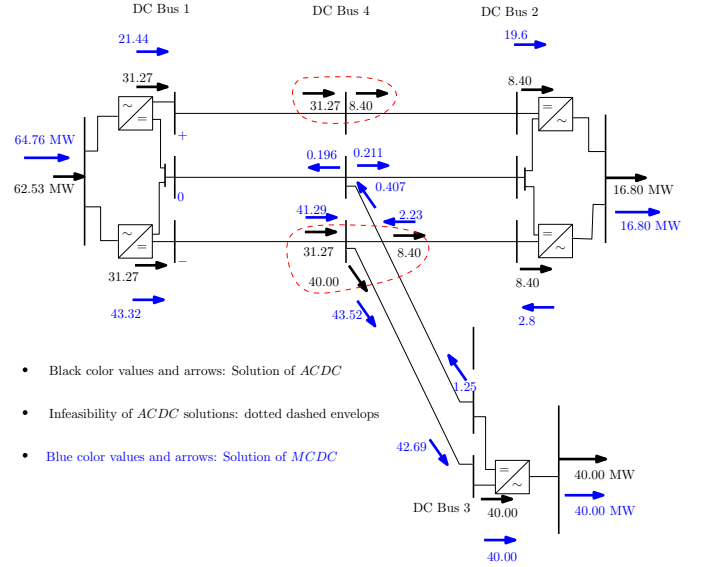


Fig. 8. Infeasibility of solutions obtained with balanced OPF model (*ACDC*) and correct solutions with the proposed unbalanced OPF model (*MCDC*)

TABLE V
POWER EXCHANGE (MW) BETWEEN AC NETWORKS AND DC NETWORK USING BALANCED OPTIMAL POWER FLOW TOOL

	Conv 1	Conv 2	Conv 3
Net Power Transfer	62.53	-16.80	-40.00
Positive Pole	31.27	-8.40	-20.00
Negative Pole	31.27	-8.40	-40.00

TABLE VI
GENERATOR DISPATCH OBTAINED BY THE BALANCED AND MULTI-CONDUCTOR MODEL

Generator	AC Bus no.	Pg (<i>ACDC</i>)	Pg (<i>MCDC</i>)
1	1	1.42883	1.42883
2	2	0.89328	0.91557
3	6	1.42882	1.42881
4	7	0.10000	0.10000
5	11	0.10000	0.10000

cases except for a slight difference in the set-point of the generator at bus 2. This difference is caused by the non-linear losses of the converters and DC branches. As the converter and line losses depend on the square of the current, the unbalanced distribution of the currents results in higher losses, which are reflected in the higher generator output.

However, the value of the proposed model is clear from the results provided in Tables VII and VIII. Table VII presents the p.u. voltage magnitudes of the positive, negative, and neutral terminals of the DC buses. Since the neutral point of converter 1 (DC bus 1) is grounded, its magnitude is zero. Due to the flow of the current through the neutral conductor, the neutral terminal voltage magnitudes at other buses take non-zero values. The positive and negative terminal voltages can also be observed to be in the constrained range of 0.9 to 1.1 pu and are pushed towards the upper (lower in the case of the negative pole) bounds to minimize the losses in the system.

The top section of Table VIII shows active power injections from the AC side to each converter pole at the corresponding

TABLE VII
VOLTAGES OVER THE TERMINAL OF DC BUSES

	DC Bus 1	DC Bus 2	DC Bus 3	DC Bus 4
Postive terminal	1.1	1.0804	-	1.0902
Negative terminal	-1.1	-1.0812	-1.0592	-1.0801
Neutral terminal	0	0.0008	-0.0311	-0.0101

TABLE VIII
VALUES OF CONVERTER VARIABLES FOR UNBALANCED OPF

Pgrid (from AC grid to conv.) MW			
	Conv 1	Conv 2	Conv 3
Positive pole	21.44	-19.6	-
Negative pole	43.32	2.8	-40.00
Pdc (from DC grid to conv.) MW			
	Conv 1	Conv 2	Conv 3
Postive terminal	-20.7	20.33	-
Negative terminal	-42.05	-2.24	42.69
Neutral terminal	0	-02.0	-1.25
Idc (DC side conv. current) pu			
	Conv 1	Conv 2	Conv 3
Postive terminal	-0.1882	0.1882	-
Negative terminal	0.3823	0.0207	-0.403
Neutral terminal	-0.1941	-0.2089	0.403

converter station. It can be observed that the power flowing through the different poles differs not only in value but also the direction (sign). Here the positive pole of Conv-2 feeds power from the DC grid to the AC grid, whereas the negative pole does the opposite creating a circulating power between the positive and negative poles (see Fig. 8). The difference in the power injection values at both ends of the DC branches (Fig. 8) is caused by the DC branch losses. The middle section of Table VIII shows the DC power output of the converters, which differs from the above values by the converter losses. The last section of Table VIII shows the current balance across the terminals of the DC converters. It can be observed that the current balance between the positive and negative poles and the neutral is conserved as intended.

E. Neutral point voltages with increasing system imbalance

The test case under study considers the values of the metallic return resistance equal to the value of pole (positive or negative) conductors. Since the metallic conductor is modeled separately, its resistance value r_{d0} can be chosen independently as per the system design and requirements. This value affects the system losses as well as the magnitudes of the neutral terminals of the DC buses. To show the impact of the metallic return conductor resistance more explicitly, its value is chosen as $r_{d0} = 10 \cdot r_{d\phi}$. Additionally, the load at AC bus 11, is varied from 0.05 pu to 0.5 pu with a step size of 0.05 pu., thus step-wise increasing unbalance in the system. For each step, the neutral terminal voltages of all DC buses and the output of generator 5 (connected at AC bus 11), are plotted in Fig. 9. It can be observed that until an unbalanced load of 0.25 pu, the output of the generator at AC bus 11 (Pg5) remains unchanged (at its lower limit of 0.1 pu). This means that the entire incremental load is supplied by the cheaper generators in the system through the DC grid. At this point, the neutral terminal voltage of DC bus 3 reaches its lower limit of -0.1 pu. Therefore, beyond this load point, Pg5 (the

most expensive generator in the system) has to be dispatched more. At a load of 0.3 pu at AC bus 11 (or DC bus 3), the neutral terminal voltage of DC bus 2 also reaches its limit (0.1 pu), which further limits the power transfer from the DC grid and yields a faster increase of the output of generator 5, indicated by the steeper slope of the curve. Thus, the flow of current over the metallic return conductor is constrained by both its resistance and neutral terminal voltages. Therefore, an explicit representation multi-conductor model is essential to capture these boundaries of the systems.

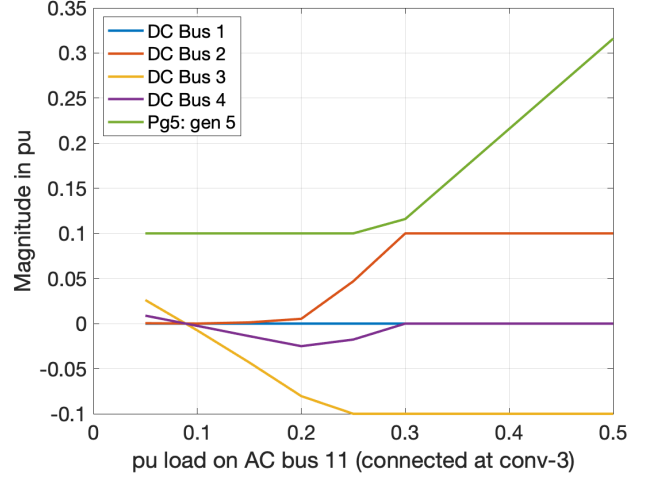


Fig. 9. Impact of the higher metallic return resistance on the neutral terminal (DC bus) voltages and active power output of generator 5 in dependence of the unbalanced load at converter 3

V. LARGER TEST CASES AND COMPUTATIONAL ANALYSIS

The test case presented in the previous section is designed to explain the proposed multi-conductor modeling and demonstrate its value in capturing the system boundaries, i.e., constraints. However, the computational cost of the added detail in the proposed multi-conductor model and the scalability of the model are analyzed in this section considering that the modelling of the HVDC substations and the DC grid require a higher number of variables and constraints. The non-linear optimization problem is solved using the Ipopt solver in Julia/JuMP environment. All simulations are performed on a machine with a “2.3 GHz 8-Core Intel Core i9” processor and “32 GB 2667 MHz DDR4” RAM.

Table IX presents the objective function values and the time taken to solve the OPF problem for test cases of different system sizes. Moreover, the DC side of all the test cases is chosen as a balanced bipolar system so that the accuracy and speed of the proposed multi-conductor model (*MCDC*) can be compared with the pre-existing single conductor model (*ACDC*, [26]). We can observe that the *MCDC* converges to the same solution (objective function value) as the balanced single conductor model up to the numerical accuracy of the solver. However, we observe that the solving time is higher than for the balanced model. Since the *MCDC* model changes only the number of variables and constraints for the DC size, the changes in problem size and solve time are also related

TABLE IX
OPF RESULTS FOR VARIOUS TEST CASES WITH BALANCED BIPOLAR CONFIGURATION

Test case	AC side		DC side		AC/DC Converters	objective value		Solve time	
	Bus	Branches	Bus	Branches		ACDC	MCDC	ACDC	MCDC
case5_2grids_MC	11	14	4	3	3	861.2947	861.2947	0.0625	0.1782
case39_mcdc	39	46	10	12	10	41,995.5127	41,995.5127	0.4204	0.9961
case67scopf_mcdc	67	102	9	11	9	86079.3816	86079.3816	0.2756	0.48069
case3120sp_acdc	3,120	3693	5	5	5	2,142,635.0308	2142635.0308	19.15552	17.88725

TABLE X
OPF RESULTS FOR THE LARGE CASES WITH UNBALANCES ON THE DC SIDE

Test case	Objective value			Outage on pole
	ACDC	MCDC	Solve time	
case5_2grids_MC	x	886.2829	0.26028	Conv-1 +Ve
case39_mcdc	x	41995.8283	1.40764	Dcline-2 -Ve
case67_mcdc	x	86169.9679	0.89440	Conv-1 -Ve
case3120sp_acdc	x	214288.1372	13.01446	Conv-2 -Ve

to the size of the DC grid. Here, the DC grid in the 67-bus test case is larger than the DC grid of the 3120-bus network. Therefore, the solution time of the 11-bus, 39-bus, and 67-bus increases to a larger extent for the unbalanced model, whereas for the 3120-bus system, it's almost the same (or a bit less). Thus, as expected, the detailed modeling comes with an additional computational cost which obviously depends on the relative size of the DC system.

Moreover, the value created by this additional cost is reflected more clearly in table X, where the balanced model fails to capture the correct operating points for the AC/DC system with an unbalanced DC grid. From this table, it can be concluded that the proposed multi-conductor model converges to a feasible optimal solution for an unbalanced system, where the source of the unbalance is mentioned as a remark. As expected, the cost of operating the system in an unbalanced state (due to the corresponding component outage) is higher than that in a balanced case.

VI. CONCLUSION

A hybrid AC/DC optimal power flow model for the unbalanced operation of HVDC grids is introduced using a multi-conductor representation of the DC grid. The positive and negative poles of bipolar converter stations are modeled separately, and DC buses are modeled using three terminals: the positive, the negative, and the neutral terminal. Each conductor of a DC branch is modeled separately, including the metallic and ground return conductors. The proposed model is implemented as a software tool in the Julia language and validated against existing balanced AC/DC grid OPF models.

It has been demonstrated that the unbalanced operation of HVDC grids cannot be correctly analyzed using balanced OPF models, as the assumption of equal power sharing among converter poles results in solutions that are infeasible when applied to the system. Further, the proposed multi-conductor representation can accurately capture such unbalances and provides converter and generator set points respecting the maximum allowable neutral terminal voltage, e.g., a maximum system unbalance. The numerical results show that in such

unbalanced models, the explicit modeling of the converter current balance using an I-V formulation is essential due to the numerical problems caused by the near-zero values of neutral voltages in (P-V) formulations.

The proposed model and implementation provide a basis that will be extended in future work to incorporate further planning and operational aspects of hybrid AC/DC grids with unbalanced DC sides.

REFERENCES

- [1] N. Flourentzou, V. G. Agelidis, and G. D. Demetriades, "Vsc-based hvdc power transmission systems: An overview," *IEEE Transactions on power electronics*, vol. 24, no. 3, pp. 592–602, 2009.
- [2] D. Van Hertem, O. Gomis-Bellmunt, and J. Liang, *HVDC grids: for offshore and supergrid of the future*. John Wiley & Sons, 2016.
- [3] E. Pierri, O. Binder, N. G. Hemdan, and M. Kurrat, "Challenges and opportunities for a european hvdc grid," *Renewable and Sustainable Energy Reviews*, vol. 70, pp. 427 – 456, 2017. [Online]. Available: <http://www.sciencedirect.com/science/article/pii/S136403211631005X>
- [4] InnoDC. Innovative tools for offshore wind and DC grids, European Union Horizon 2020 research and innovation programme, Project ID: 765585. <http://innodc.org/>.
- [5] Best Paths. Beyond state-of-the-art technologies for power AC corridors and multi-terminal HVDC systems, European Union Horizon 2020 research and innovation programme, project ID: 612748. <http://www.bestpaths-project.eu/>.
- [6] J. Beerten, S. Cole, and R. Belmans, "Generalized steady-state vsc mtcd model for sequential ac/dc power flow algorithms," *IEEE Transactions on Power Systems*, vol. 27, no. 2, pp. 821–829, 2012.
- [7] R. Wiget and G. Andersson, "Optimal power flow for combined ac and multi-terminal hvdc grids based on vsc converters," in *2012 IEEE Power and Energy Society General Meeting*, July 2012, pp. 1–8.
- [8] J. Rimez and R. Belmans, "A combined ac/dc optimal power flow algorithm for meshed ac and dc networks linked by vsc converters," *International Transactions on Electrical Energy Systems*, vol. 25, no. 10, pp. 2024–2035, 2015.
- [9] L. Gan and S. H. Low, "Optimal power flow in direct current networks," *IEEE Transactions on Power Systems*, vol. 29, no. 6, pp. 2892–2904, Nov 2014.
- [10] J. Beerten and R. Belmans, "Development of an open source power flow software for high voltage direct current grids and hybrid ac/dc systems: Matakdc," *IET Generation, Transmission & Distribution*, vol. 9, no. 10, pp. 966–974, 2015.
- [11] N. Meyer-Huebner, M. Suriyah, and T. Leibfried, "Distributed optimal power flow in hybrid ac–dc grids," *IEEE Transactions on Power Systems*, vol. 34, no. 4, pp. 2937–2946, 2019.
- [12] A. Mešanović, U. Muenz, and C. Ebenbauer, "Robust optimal power flow for mixed ac/dc transmission systems with volatile renewables," *IEEE Transactions on Power Systems*, vol. 33, no. 5, pp. 5171–5182, 2018.
- [13] M. Hotz and W. Utschick, "hynet: An optimal power flow framework for hybrid ac/dc power systems," *IEEE Transactions on Power Systems*, vol. 35, no. 2, pp. 1036–1047, 2019.
- [14] H. Ergun, J. Dave, D. Van Hertem, and F. Geth, "Optimal power flow for ac–dc grids: Formulation, convex relaxation, linear approximation, and implementation," *IEEE Transactions on Power Systems*, vol. 34, no. 4, pp. 2980–2990, July 2019.
- [15] J. Dave, H. Ergun, T. An, J. Lu, and D. Van Hertem, "TNPEP of meshed HVDC grids: AC, DC and convex formulations," *IET Generation, Transmission & Distribution*, vol. 13, no. 24, pp. 5523–5532, 2019.

- [16] A. Elahidoost and E. Tedeschi, "Expansion of offshore hvdc grids: An overview of contributions, status, challenges and perspectives," in *2017 IEEE 58th International Scientific Conference on Power and Electrical Engineering of Riga Technical University (RTUCON)*. IEEE, 2017, pp. 1–7.
- [17] A. H. Dominguez, L. H. Macedo, A. H. Escobar *et al.*, "Multistage security-constrained HVDC/HVAC transmission expansion planning with a reduced search space," *IEEE Trans. on Power Systems*, vol. 32, no. 6, pp. 4805–4817, 2017.
- [18] L. Guo, Y. Ding, M. Bao, C. Shao, P. Wang, and L. Goel, "Nodal reliability evaluation for a vsc-mtde-based hybrid ac/dc power system," *IEEE Transactions on Power Systems*, vol. 35, no. 3, pp. 2300–2312, 2019.
- [19] D. Van Hertem, W. Leterme, G. Chaffey, M. Abedrabbo, M. Wang, F. Zerihun, and M. Barnes, "Substations for Future HVdc Grids: Equipment and Configurations for Connection of HVdc Network Elements," *IEEE Power and Energy Magazine*, vol. 17, no. 4, pp. 56–66, July 2019.
- [20] T.-H. Chen, M.-S. Chen, K.-J. Hwang, P. Kotas, and E. A. Chebli, "Distribution system power flow analysis—a rigid approach," *IEEE Transactions on Power Delivery*, vol. 6, no. 3, pp. 1146–1152, 1991.
- [21] C. S. Cheng and D. Shirmohammadi, "A three-phase power flow method for real-time distribution system analysis," *IEEE Transactions on Power Systems*, vol. 10, no. 2, pp. 671–679, 1995.
- [22] F. Geth, S. Claeys, and G. Deconinck, "Current-voltage formulation of the unbalanced optimal power flow problem," in *2020 8th Workshop on Modeling and Simulation of Cyber-Physical Energy Systems*. IEEE, 2020, pp. 1–6.
- [23] F. Geth and H. Ergun, "Real-Value Power-Voltage Formulations of, and Bounds for, Three-Wire Unbalanced Optimal Power Flow," *arXiv preprint arXiv:2106.06186*, 2021.
- [24] L. Mackay, A. Dimou, R. Guarnotta, G. Morales-Espania, L. Ramirez-Elizondo, and P. Bauer, "Optimal power flow in bipolar dc distribution grids with asymmetric loading," in *2016 IEEE International Energy Conference (ENERGYCON)*, April 2016, pp. 1–6.
- [25] L. Mackay, R. Guarnotta, A. Dimou, G. Morales-Espania, L. Ramirez-Elizondo, and P. Bauer, "Optimal power flow for unbalanced bipolar dc distribution grids," *IEEE Access*, vol. 6, pp. 5199–5207, 2018.
- [26] H. Ergun. (2019) Powermodelsacdc.jl version 1.0. [Online]. Available: <https://github.com/hakanergun/PowerModelsACDC.jl>
- [27] I. Dunning, J. Huchette, and M. Lubin, "JuMP: A modeling language for mathematical optimization," *SIAM Review*, vol. 59, no. 2, pp. 295–320, 2017.
- [28] C. Coffrin, R. Bent, K. Sundar, Y. Ng, and M. Lubin, "PowerModels.jl: An Open-Source Framework for Exploring Power Flow Formulations," in *2018 Power Systems Computation Conference (PSCC)*, June 2018, pp. 1–8.
- [29] D. M. Fobes, S. Claeys, F. Geth, and C. Coffrin, "Powermodelsdistribution.jl: An open-source framework for exploring distribution power flow formulations," *Electric Power Systems Research*, vol. 189, p. 106664, 2020. [Online]. Available: <http://www.sciencedirect.com/science/article/pii/S0378779620304673>
- [30] W. Leterme, P. Tielens, S. De Boeck, and D. Van Hertem, "Overview of grounding and configuration options for meshed hvdc grids," *IEEE Transactions on Power Delivery*, vol. 29, no. 6, pp. 2467–2475, Dec 2014.
- [31] D. K. Molzahn, I. A. Hiskens *et al.*, "A survey of relaxations and approximations of the power flow equations," *Foundations and Trends® in Electric Energy Systems*, vol. 4, no. 1-2, pp. 1–221, 2019.